FEATURE ARTICLE

Controlled Chemical Routes to Nanotube Architectures, Physics, and Devices

Hongjie Dai,* Jing Kong, Chongwu Zhou, Nathan Franklin, Thomas Tombler, Alan Cassell, Shoushan Fan, and Michael Chapline

Department of Chemistry, Stanford University, Stanford, California 94305

Received: July 12, 1999; In Final Form: October 21, 1999

This article presents our recent work in the controlled synthesis of multiwalled (MWNT) and single-walled nanotubes (SWNT) with ordered architectures. The general synthesis approach involves chemical vapor deposition using rationally designed catalyst and substrates. The results include self-oriented MWNTs, individual SWNTs grown from controlled surface sites, and structures of suspended SWNTs along well-defined directions. The chemically derived nanotube architectures have opened up new possibilities in fundamental characterization and potential applications of nanotube materials. Systematic electron transport measurements are carried out to elucidate the electrical properties of various classes of SWNTs and to explore the physics in one-dimensional systems. High-performance electrical devices based on individual SWNTs are enabled by combining synthesis and microfabrication approaches.

Introduction

Carbon nanotubes exhibit intriguing and potentially useful structural, electrical, and mechanical properties.[1−4] A nanotube has high Young's modulus and tensile strength and can be metallic, semiconducting, or semimetallic depending on the helicity and diameter. Utilization of these properties with individual or ensembles of nanotubes have led to advanced scanning probes,[5−9] nanoelectronic devices,[10−12] and electron field emission sources.[13−18]

Developing controlled synthesis methods to obtain ordered carbon nanotube architectures is an important and viable route to fundamental characterization and potential applications of novel molecular wires. The ultimate goal in nanotube synthesis should be the gain of control over the locations and orientations of nanotubes, as well as their atomic structures including helicity, diameter, and topological defects. In recent years, significant progress has been made in controlling the growth of multiwalled carbon nanotubes (MWNTs)[19] on surfaces using chemical vapor deposition (CVD) methods. Long and well-aligned MWNTs on large-scale substrates have been synthesized.[18,20−22] However, the growth of single-walled nanotubes (SWNTs)[23] into ordered architectures remains a challenging task.

This paper presents our development of controlled CVD synthesis strategies to obtain ordered multiwalled and single-walled nanotube structures. The key elements in our overall approach include understanding the chemistry of catalyst materials and synthesizing nanotubes on rationally designed substrates containing patterned catalyst. The results include MWNTs self-oriented perpendicular to substrates and assembled into regular arrays. By enabling a CVD synthesis method for structurally perfect SWNTs, individual SWNTs are grown from controlled surface sites. Also, for the first time, suspended SWNT architectures with nanotubes directed toward well-defined orientations are synthesized.

The nanotube architectures derived by controlled chemical routes have opened up new possibilities in fundamental characterization and potential applications of novel nanowire materials. In particular, single-walled nanotubes are true molecular wires with their diameters in such a regime (∼1−5 nm) that the electronic structure of a SWNT sensitively depends on its chirality.[1] SWNTs serve as ideal systems to study physics problems in quasi one dimension. To this end, we will show that our growth strategy readily allows SWNTs to be integrated into electrical circuits and addressed individually. Systematic electron transport measurements are carried out to elucidate the electrical properties of various classes of nanotubes. Also, high gain field-effect transistors based on individual SWNTs are demonstrated.

Synthetic Strategies for Various Nanotube Architectures

Growth of Self-Oriented Multiwalled Nanotubes. Previous methods to obtain ordered multiwalled nanotube structures relied on the CVD growth of nanotubes in confined environments including the pores of mesoporous silica or channels of alumina membranes.[20,21,24,25] We found that nanotubes can self-assemble into aligned structures during CVD growth, and the driving force for self-alignment is the van der Waals interactions between nanotubes.[18] Our synthesis approach involved catalyst patterning and rational design of the substrate to enhance catalyst−substrate interactions and to control the catalyst particle size. The substrates were porous silicon obtained by electrochemical etching of n-type silicon wafers in HF/methanol solutions. The resulting substrate consisted of a thin nanoporous layer (pore size of ∼3 nm) on top of a macroporous layer (with submicrometer pores).[26,27] Patterned catalyst squares on the porous silicon substrate were obtained by evaporating a 5 nm thick iron film through a shadow mask. CVD growth using the substrate was then carried out at 700 °C in a 2-in. tube furnace under an ethylene flow of 1000 sccm/min for 15−60 min. Figure

10.1021/jp992328o CCC: $18.00 © 1999 American Chemical Society
Published on Web 12/07/1999

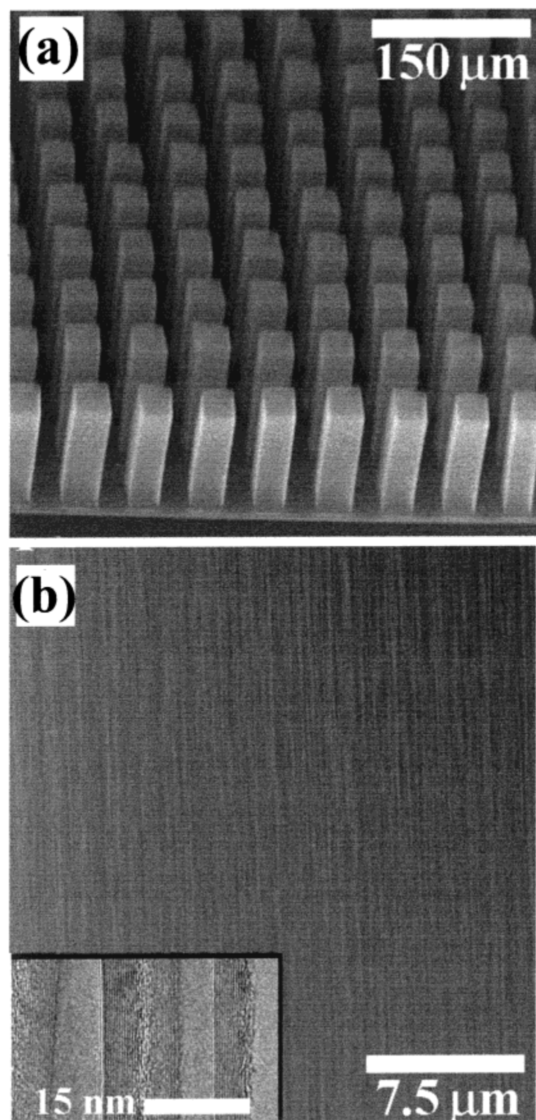

Figure 1. (a) Scanning electron microscopy image of arrays of bundled multiwalled nanotube towers. (b) High-resolution SEM showing aligned MWNTs within a tower. The inset shows a TEM image of the bundled MWNTs.

1a shows a scanning electron microscope (SEM) image of regularly spaced arrays of nanotube towers grown on top of patterned iron squares on porous silicon substrates. The nanotube towers exhibit very sharp edges and corners with no nanotubes branching away from the blocks. The high-resolution SEM image (Figure 1b) reveals that the MWNTs (Figure 1b inset) within each block are well aligned along the direction perpendicular to the substrate surface. The length of the nanotubes and thus the height of the towers can be controlled in the range 10–240 μm by varying the CVD reaction time, and the width of the towers is controlled by the size of the openings in the shallow mask. The smallest self-oriented nanotube towers synthesized by our method are 2 μm $\times$ 2 μm wide.

The mechanism of nanotube self-orientation involves the nanotube base growth mode.[18] Since the nanoporous layer on the porous silicon substrate serves as an excellent catalyst support, the iron catalyst nanoparticles formed on the nanoporous layer interact strongly with the substrate and remain pinned on the surface. During CVD growth, the outermost walls of nanotubes interact with their neighbors via van der Waals forces to form a rigid bundle, which allows the growth of nanotubes perpendicular to the substrate. The porous silicon substrates exhibit important advantages over plain silicon substrates in the synthesis of self-aligned nanotubes. Growth on substrates containing both porous silicon and plain silicon portions find that nanotubes grow at a higher rate (in length/min) on porous silicon than on plain silicon. This result suggests that ethylene molecules can permeate through the macroporous silicon layer and thus efficiently feed the growth of inner and outer nanotubes within the towers. The nanotubes grown on porous silicon substrates exhibit monodispersed diameters, since catalyst nanoparticles with a narrow size distribution can be formed on the porous supporting surface and the strong catalyst–support interactions prevent the catalyst particles from sintering at elevated temperatures during CVD growth.

Enabling the Growth of Single-Walled Nanotubes by CVD. Arc discharge[28,29] and laser ablation[30] have been the principal methods for obtaining high-quality single-walled nanotube materials. Both methods involve evaporating carbon atoms from solid carbon sources at ≥3000 °C, which limits the scale-up of SWNTs. Also, nanotubes synthesized by the evaporation methods are in tangled forms that are difficult to purify, manipulate, and assemble for building addressable nanotube architectures. Chemical vapor deposition methods have been very successful in synthesizing carbon fibers, filaments, and MWNTs.[31–35] However, CVD synthesis of high-quality SWNTs is only recent by using methane as carbon feedstock and iron oxide nanoparticles supported on high surface area alumina as the catalyst.[36] High-temperature conditions (850–1000 °C) are employed in the growth to overcome high strain energies in forming small diameter SWNTs (<5 nm), and to obtain nearly defect-free tube structures. The choice of methane is critical to the CVD approach to SWNTs. It is found that methane is stable at the elevated growth temperatures without appreciable self-pyrolysis. This stability prevents the formation of amorphous carbon that tends to cause catalyst poisoning and overcoating of the nanotubes. Catalytic decomposition of methane by the transition metal catalyst particles is thus the dominant process in SWNT growth.[36–38]

Within the methane CVD approach, we find that the chemical and textural properties of the catalyst materials dictate the yield and quality of SWNTs.[38] Bulk quantities of high-quality single-walled carbon nanotubes (SWNTs) can be synthesized by optimizing the catalyst. Thus far, our optimized catalyst consists of Fe/Mo bimetallic species supported on a sol–gel derived alumina–silica multicomponent material.[38] Shown in Figure 2 is a TEM image of SWNTs synthesized in bulk by using this catalyst. The image illustrates the remarkable abundance of individual and bundled SWNTs that are free of defects and amorphous carbon coating. The diameters of the SWNTs are dispersed in the range 0.7–5 nm with a peak at 1.7 nm. Weight gain studies found that the yield of nanotubes can be as high as 45 wt %. Through systematic studies, we have found that a good catalyst material for SWNT synthesis necessarily exhibits strong metal–support interactions, possesses a high surface area and large pore volume, and retains these characteristics at high temperatures without sintering. The strong metal–support interactions allow high metal dispersion and thus a high density of catalytic sites. The open pore structure of a catalyst allows efficient diffusion of reactant and intermediate hydrocarbon species. We believe that the rate-limiting step in SWNT CVD growth involves gas diffusion. This is based on the results that high-SWNT-yielding catalysts exhibit large pore volumes in the mesopore regime.

Growth Mechanism of SWNT. The states of nanotube ends contain rich information about nanotube growth mechanisms.

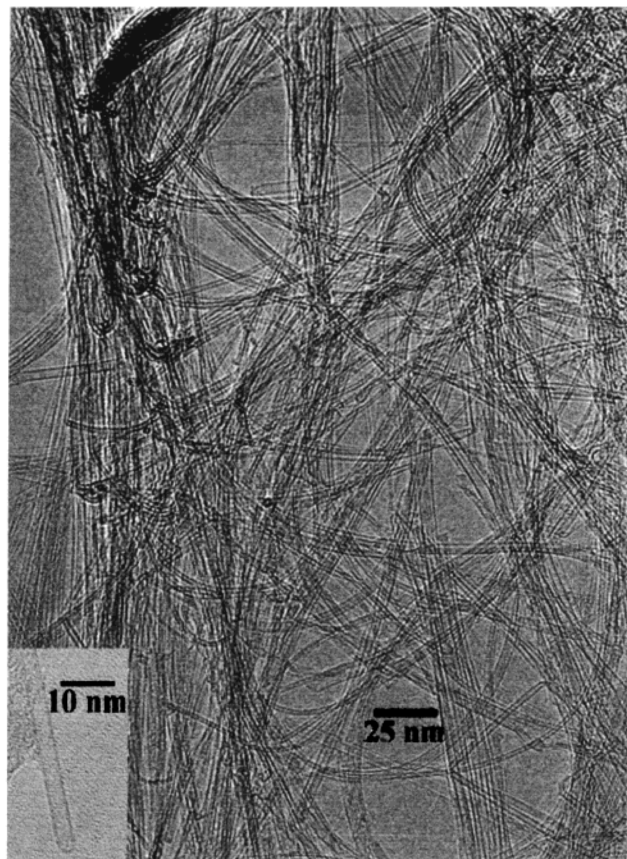

Figure 2. TEM image of SWNTs synthesized in bulk using a catalyst supported on a sol–gel derived alumina–silica hybrid material. Inset: an example of the frequently observed SWNT ends that are closed and free of metal particles.

Careful high-resolution TEM imaging of the SWNTs synthesized by our CVD method frequently observes closed tube ends that are free of attached or encapsulated metal particles (Figure 2 inset). The opposite ends are typically found embedded in the catalyst support particles when imaged along the lengths of the nanotubes. These observations suggest that SWNTs grow in the methane CVD process predominantly via the base growth process.[31,32,36–42] The first step of the CVD reaction involves the absorption and decomposition of methane molecules on the surface of transition metal catalytic nanoparticles on the support surface. Subsequently, carbon atoms dissolve and diffuse into the nanoparticle interior to form a metal–carbon solid-state solution. Nanotube growth occurs when supersaturation leads to carbon precipitating into a crystalline tubular form. The size of the metal catalyst nanoparticle generally dictates the diameter of the synthesized nanotube. In the base growth mode, the nanotube lengthens with a closed end while the catalyst particle remains on the support surface. Carbon feedstock is thus supplied from the "base" where the nanotube interfaces with the anchored metal catalyst. Base growth operates when strong metal–support interactions exist so that the metal species remain pinned on the support surface. In contrast, in the tip growth mechanism, the nanotube lengthening involves the catalyst particle lifting off from the support and carried along at the tube end. The carried-along particle is responsible for supplying carbon feedstock needed for the tube growth.[31,32,39–41] This mode operates when the metal–support interaction is weak. In the methane CVD method, we find that enhancing metal–support interactions leads to significant improvement in the performance of the catalyst material in producing high-yield SWNTs. This is rationalized by the increased catalytic sites and the facilitated base-mode growth processes. On the other hand, catalysts with weak metal–support interactions lead to aggregation of metal species and reduced nanotube yield and purity.[38] Further understanding of the chemistry of catalysts and nanotube growth will undoubtedly lead to the synthesis of bulk quantities of high-quality SWNTs approaching the kilogram scale.

Growth of Isolated Single-Walled Nanotubes on Controlled Surface Sites. The successful CVD synthesis of SWNTs in bulk forms has led to a straightforward synthetic route to addressable individual nanotube wires. By using substrates patterned with 1–5 μm wide catalytic islands, we obtain "nanotube chips" that contain isolated single-walled nanotubes grown from desired locations on the substrates.[12,37,43] Atomic force microscopy (AFM) images of SWNTs on a nanotube chip is shown in Figure 3, where the synthesized nanotubes extending from the catalyst islands are clearly observed. The diameters of the nanotubes are measured to be in the range 0.7–4.0 nm, which is consistent with TEM results obtained with bulk SWNT materials. Some of the nanotubes have one end attached to a catalyst island and the other end terminated between islands. Nanotubes bridging islands with both ends attached to the opposing islands are also observed. As described in a later section, the bridging SWNTs allow reliable electrical connections to be made from the macroscopic scale to individual SWNTs. Thus, our controlled chemical synthesis opens up a new route to individual nanowire electrical circuits that are needed for fundamental and practical purposes.

Growth of Free-Standing SWNTs with Directed Orientations. Obtaining single-walled carbon nanotube architectures with nanotubes in aligned orientations has been challenging. We have devised a synthesis strategy that leads to suspended SWNTs directed toward controlled orientations parallel to the plane of a silicon substrate. The SWNTs are suspended bridges grown from catalyst material placed on top of regularly patterned silicon tower structures.[68] The synthesis approach begins with developing a series of liquid-phase catalyst precursor materials that allow for uniform film formation and large-scale catalyst patterning. A specific precursor material consists of ethanol (40 mL) and 2-butanol (20 mL) solutions of P-123 block copolymer (1. 0 g),[44,45] $AlCl_3 \cdot 6H_2O$ (2.4 g), $FeCl_3 \cdot 6H_2O$ (0.09 g), and MoO_2Cl_2 (0.004 g). Using contact printing[46,47] of a flat polydimethylsiloxane (PDMS) stamp inked with a film of the precursor material, we selectively place the precursor on top of tower arrays premade on a silicon substrate. Calcination at 700 °C for 4 h leads to the formation of catalytic iron oxide nanoparticles supported on alumina/silica mixed oxides confined on the tower tops. Subsequent CVD growth with the substrate yields SWNTs emanating from the towers. Directed free-standing SWNT networks are formed by nanotubes growing to adjacent towers and suspended above the surface. When examining with a scanning electron microscope (SEM), we observe that highly directional suspended SWNTs are formed on the synthesized sample. The directions of the suspended tubes are determined by the pattern of the towers. Well-aligned SWNT bridges are obtained in an area of the substrate containing isolated rows of towers as shown in Figure 4a, where suspended tubes forming a power-line-like structure can be seen. In an area containing towers in a square configuration, a square of suspended nanotube bridges is obtained (Figure 4b). Directionality of the suspended tubes is simply a result of the rationally designed substrate. During the CVD growth, nanotubes emanate from the top of the towers. The nanotubes growing toward

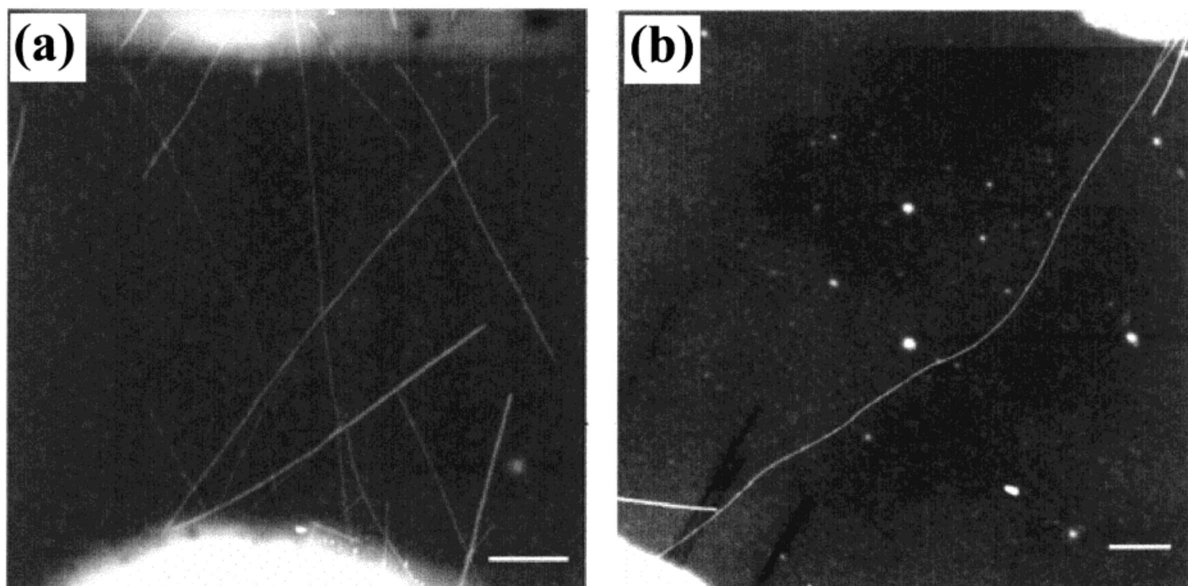

Figure 3. (a) AFM image of SWNTs grown from patterned catalyst islands on a silicon oxide substrate (scale bar: 0.5 μm). (b) Image of an individual SWNT bridging adjacent islands (scale bar: 0.5 μm).

adjacent towers become suspended, whereas nanotubes directed toward other orientations fall onto the sidewalls of the towers (not easily resolved under SEM). In Figure 4c, we show a TEM image of a suspended SWNT bridge between silicon towers and an image (Figure 4c inset) showing the high-resolution structure of the SWNT.

The directed growth of suspended SWNTs presented here involves developing a new type of liquid-phase catalyst material, contact printing of catalyst onto designed substrates and CVD synthesis. The method should open a new window in characterization and device applications of organized nanowire architectures in suspended states or after being transferred onto flat substrates.

Physics of Atomically Well-Defined Nanowires

It is well recognized that single-walled carbon nanotubes are ideal systems for studying solid-state physics in quasi one dimension.[1] SWNT wires have well-defined atomic structures and can be considered as molecule-like wires.[4] It has been actively pursued to elucidate their band structures,[1,48−52] quantum confinement,[53−55] and electron−electron[56−59] and electron−lattice[60,61] interaction effects in SWNTs. The remarkable sensitivity of a SWNT electronic structure on tube chirality and diameter requires addressing individual nanotubes in order to understand electron transport in various classes of nanotubes. Single-"molecule" transport studies are needed in order to study physical phenomena and properties that maybe averaged out in an ensemble of nanotubes. Previous approaches to addressable SWNT electrical architectures include randomly depositing SWNTs from liquid suspensions onto predefined electrodes[53] or onto a flat substrate followed by locating nanotubes and patterning electrodes.[57] Results obtained with individual single-walled tubes and ropes include Coulomb charging[56,57] and Luttinger liquid behavior[57] in metallic tubes. Semiconducting SWNTs were found to exhibit field-effect transistor characteristics at room temperature.[10−12,43] Nevertheless, the intrinsic electrical properties of various classes of nanotubes remain to be fully explored.

Integrated Circuits of Individual Single-Walled Nantubes. The synthesis of individual SWNTs at desired surface sites has enabled a controlled route to addressable SWNTs for systematic electrical measurements of nanotubes. With the SWNT chips described earlier, integrated nanotube circuits can be constructed by using a straightforward microfabrication procedure.[12,43] Various types of metals are used to contact nanotubes including Ti, Ni, Nb, Cr, Au, Al, Ag, Ca, and Mg. The contacting process places metal electrodes to fully cover the catalyst islands and extend over the edges by 0.5−1 μm. The individual SWNT bridges between islands leads to a significant number of metal−SWNT−metal electrical devices. Optical and AFM images of a representative device are shown in Figure 5. In our samples, the lengths of individual SWNTs between electrodes were ≥ 3 μm. Degenerately doped silicon wafers with 500 nm thick thermally grown oxide on the surfaces are used as substrates. The heavily doped substrate is conducting at low temperatures and used as a back-gate. Figure 5c shows the schematic structure of our devices.

Electron Transport Properties of Metallic Nanotubes. Single-walled armchair nanotubes with (n,n) indices are true metallic wires with finite density of states at the Fermi level.[1] At low temperatures, a perfect (n,n) arm-chair tube should be conducting, and transport along the length of the tube is expected to be ballistic due to quenched phonon modes and the defect- and impurity-free nature of the nanotube. If ohmic contacts can be made between metal electrodes and the tube, a resistance of 6.5 kΩ, i.e., half of the resistance quantum h/e^2, is expected.[62] However, it has been challenging to make good electrical contacts to SWNTs. At low temperatures, Coulomb blockade has been observed in individual metallic single-walled tubes or ropes because of high contact resistance on the order of megaohms. Coulomb charging effects have been the main physics studied in these samples.[56,57]

Using the approach of controlled SWNT synthesis and contacting, we have obtained a large number of low-resistance individual SWNT samples in the range of tens to hundreds of kilo-ohms (length between the edges of contacting electrodes ≥ 3 μm). These individual SWNT samples remain to be in low resistance states when cooled to low temperatures. The lowest single-tube resistance is $\sim$12 kΩ measured at 2 K. Detailed transport data obtained with this sample are shown in Figure 6. The linear resistance of the sample decreases as the temperature is decreased, and a slight upturn is observed below 30 K in the

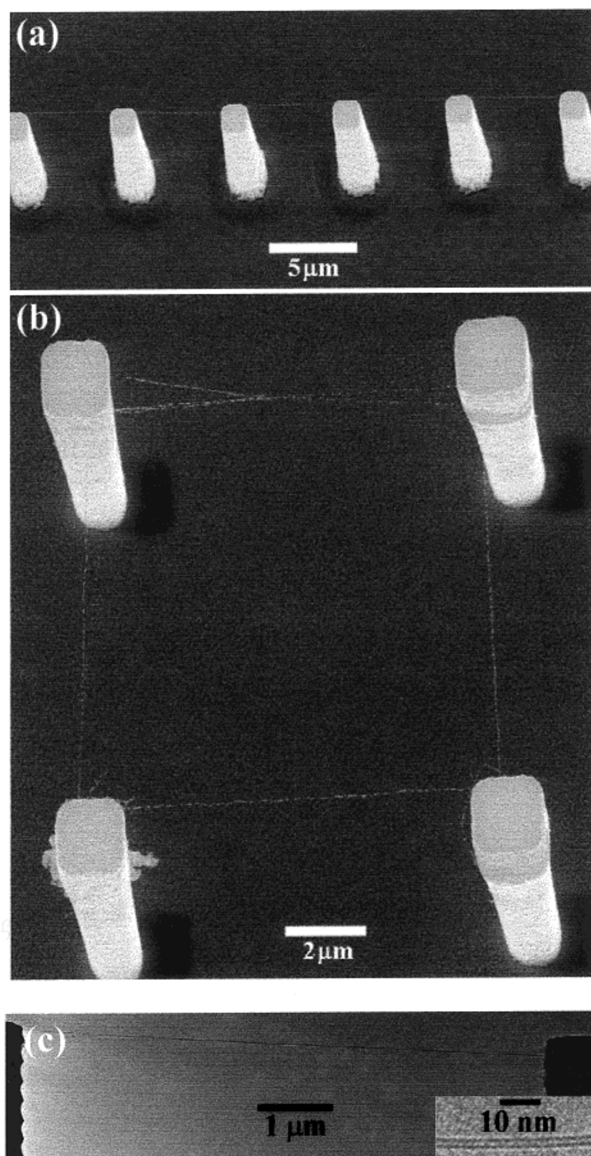

Figure 4. (a) SEM image of a suspended SWNT "power-line" structure. (b) SEM image of a square of suspended SWNT bridges. (c) TEM image of a SWNT bridge suspended between silicon towers (inset: a high-magnification TEM image showing the structure of a SWNT).

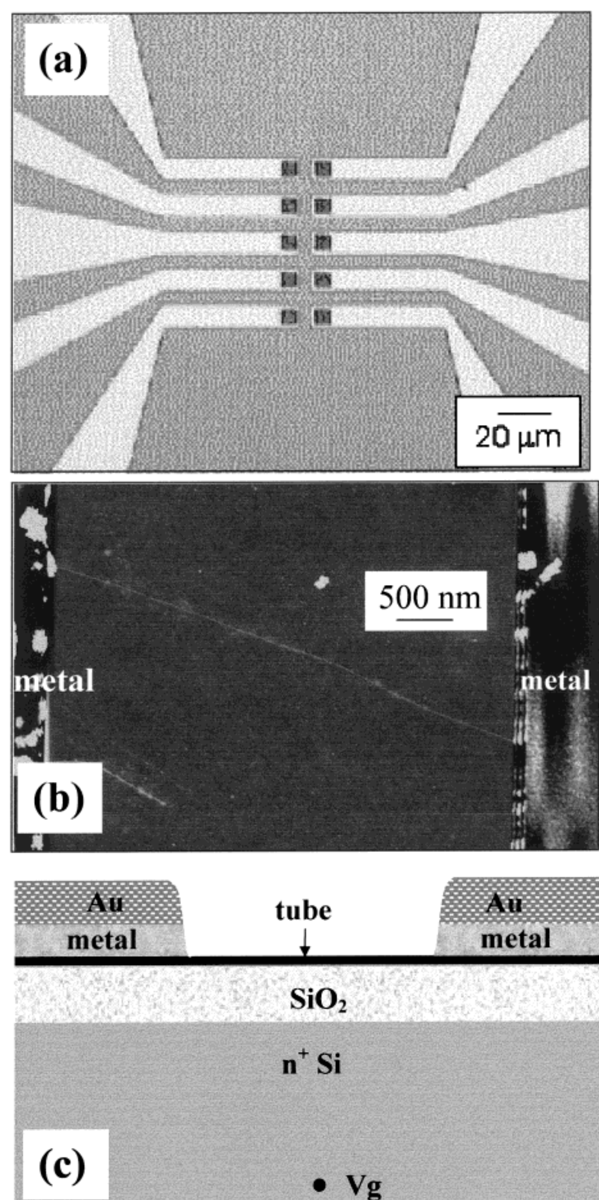

Figure 5. (a) Optical image of SWNT integrated circuits. (b) AFM image of an individual SWNT device. (c) Schematic view of the device structure.

resistance vs temperature curve (solid line in Figure 6a, measured under zero gate voltage). Applying a −10 V gate voltage is found to lower the resistance of the sample (dashed line in Figure 6a), and the resistance is 12 kΩ at 2 K. As shown in Figure 6b, current-voltage $I-V$ curves recorded under $V_g = -10$ V at room temperature and 4K exhibit linear characteristics near zero bias voltage. At 2 K, the sample exhibits clear staircase structures in the $I-V$ (dotted line in Figure 6b). However, the origin of these interesting features remains unclear at the present time. In Figure 6c, current vs gate voltage curves measured under various bias voltages show fluctuations but the absence of periodic Coulomb oscillations. Sweeping the gate voltage from −100 to 100 V, we find that the sample remains conducting in the entire experimentally accessible gate voltage range. These results suggest that the SWNT is of true metallic nature and should correspond to a (n,n) armchair tube. Coulomb blockade behavior is not clearly observed with this sample because highly transparent contacts have been made to the nanotube.

Among the various contacting metals investigated for SWNTs including Ti, Ni, Nb, Cr, Au, Al, and Ag, we have found that Ti tends to give rise to the lowest contact resistance. The low resistance is also attributed to the controlled approach of nanotube growth and integration that allow metal electrodes coupling to the sides and the ends of a nanotube. It is expected that the broken translational symmetry at a nanotube end allows strong electrical coupling between the nanotube and a metal,[63] which could be a factor in the observed low contact resistance of our samples. It remains a challenge, however, to address the precise nature of the contacts and to achieve the 6.5 kΩ resistance limit in metallic SWNT systems.

It is a common observation with our samples that upon varying gate voltage, the resistance of metallic SWNTs can be changed by a factor of 2−4. This gate dependence is far from negligible although much weaker than semiconducting SWNTs.[10−12] We attribute this phenomenon to the observation that the transparency of metal-tube contacts (or junctions) is tunable by gate voltages. This is based on recent experiments

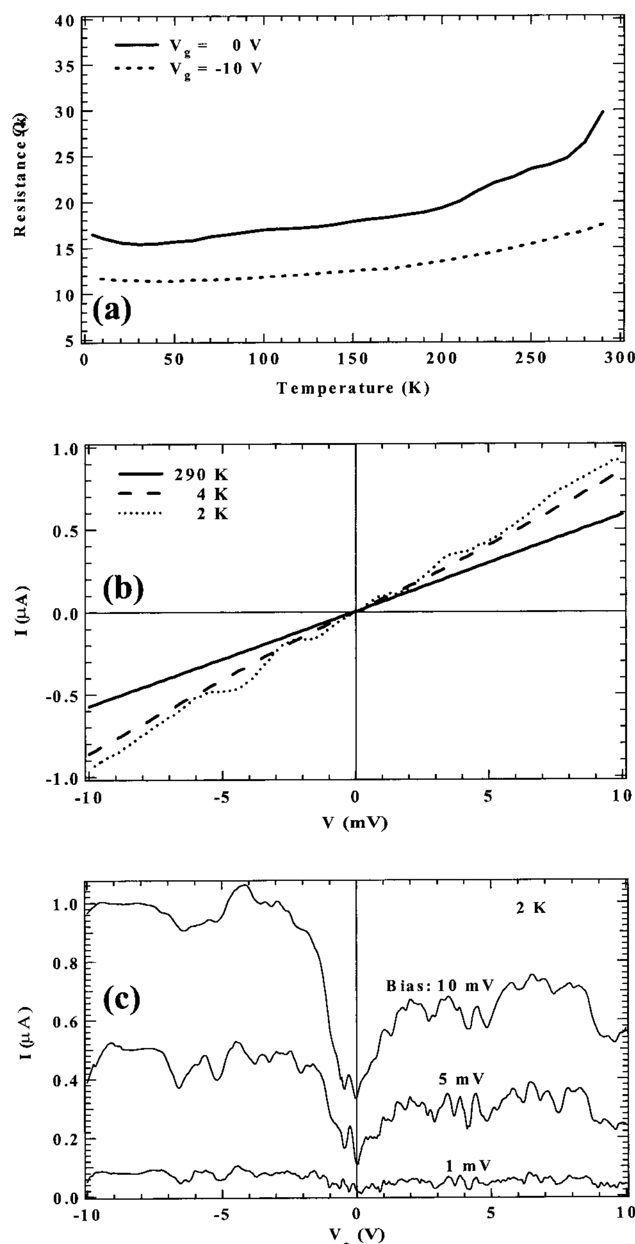

Figure 6. (a) Resistance vs temperature $R(T)$ for a metallic SWNT contacted by 20 nm/60 nm Ti/Au: (solid line) $R(T)$ measured under zero gate voltage; (dashed line) $R(T)$ measured under −10 V gate voltage. (b) $I-V$ curves recorded at 300, 4, and 2 K respectively (gate voltage = −10 V). (c) Current vs gate voltage curve recorded at 2 K under various bias voltages.

that observed superconducting proximity effect in SWNT samples in contact with superconducting Nb electrodes.[64] In this case, only under certain gate voltages are pronounced proximity effects observable, suggesting enhanced metal-tube contact transparency by these gate voltages.[64] The gate dependence of metal-tube coupling is also consistent with recent numerical calculations that found contact resistance to a SWNT depending on the Fermi energy of the tube.[67] The origin of nonperiodic fluctuations in the current vs gate voltage data for the metallic SWNT (Figure 6c) at low temperatures remains to be fully understood. Some of the variations could be due to metal-tube transparency changes under various gate voltages.

Electron Transport Properties of Semiconducting Nanotubes. Chiral (m,n) SWNTs with $m - n \neq 3 \times$ (integer) are semiconducting in nature and have primary energy gaps $E_g \propto 1/d$ where d is the nanotube diameter.[1] Transport studies of this class of nanotubes have been limited at 300 K, and temperature-dependent electrical properties remain unexplored so far.[10,11] Furthermore, fundamental issues such as the origin of carrier type, nature of contact, and transport mechanisms in semiconducting SWNTs have not been addressed. Our growth method produces SWNTs with diameters dispersed in the range ∼0.7−3 nm, and the resulting semiconducting tubes have energy gaps ∼1−0.25 eV according to band structure calculations.[1] For the first time, we have obtained temperature-dependent transport characteristics of individual semiconducting SWNTs of various tube diameters. Also, transport mechanisms through semiconducting SWNTs at various temperatures are elucidated.

We find that semiconducting SWNT samples exhibit common characteristics but differ quantitatively. The room temperature resistance is typically in the range 200−500 kΩ for samples with relatively large diameter (d > 2.0 nm) tubes. Smaller diameter tube samples with $d \leq 1.5$ nm exhibit higher resistance on the order of megaohms or higher. The semiconducting tubes appear to be hole-doped, and their conductance can be diminished by applying positive gate voltages. At 4 K, the samples are insulating and show a gaplike region within ±10 to ±1000 mV in the $I-V$ curves. The gap region is found to be larger for smaller diameter tubes. Temperature-dependent resistance of the samples shows that transport through the semiconducing tubes involves thermal activation with higher barriers for smaller diameter tubes.

Parts a and b of Figure 7 show the room-temperature $I-V$ curves obtained with a $d = 2.8$ nm and length of ∼3 µm semiconducting SWNT (sample S1). The sample exhibits a highly linear $I-V$ with a resistance of ∼370 kΩ measured at zero gate voltage. Positive gate voltages progressively reduce the linear conductance of the sample (Figure 7a). At $V_g > 3$ V, the conductance is suppressed by 4 orders of magnitude from that at $V_g = 0$. These $I-V$ characteristics are signatures of hole-doped semiconducting SWNTs acting as p-type "transistors" as reported previously.[10−12,43] The result of resistance vs temperature measured by using near-zero bias voltages ($|V| \leq$ 1 mV) under zero gate voltage is shown in the inset of Figure 7b. The temperature dependence of resistance is weak from 300 to 25 K, with an increase from 370 kΩ to 1 MΩ. Below 25 K, the resistance increases sharply and $R(T)$ can be approximately fitted to $\exp[-E_a/(k_BT)]$ with an activation barrier of $E_a \approx 4.6$ meV (Figure 7b inset). At 4 K, a gap of ∼20 mV is observed in the $I-V$ curve and the sample is insulating in the bias range $|V| \lesssim 10$ mV (Figure 7b). The insulating region is found to be significantly suppressed by applying a − 1.5 V gate voltage. On the other hand, applying a positive gate voltage leads to a larger insulating region in the $I-V$ curve (Figure 7b).

In parts c and d of Figure 7, we show the results obtained with a $d = 1.3$ nm and length of ∼5 µm semiconducting SWNT (sample S2). The room-temperature linear resistance of the sample is ∼3.4 MΩ under zero gate and is dramatically increased by positive gate voltages (Figure 7c inset). When the sample is cooled, the $I-V$ curve becomes nonlinear and the resistance is infinity below 40 K because of the appearance of a gaplike insulating region in $I-V$. At 4 K, the insulating region is within ±0.7 V as shown in Figure 7c. The linear resistance of the sample sharply increases as temperature decreases and can be well fitted into an exponential form $R(T) \approx \exp[-E_a/(k_BT)]$ with an activation barrier $E_a \approx 25$ meV (Figure 7d).

A band diagram model is presented in Figure 8 for a metal−semiconducting tube−metal system to rationalize the obtained

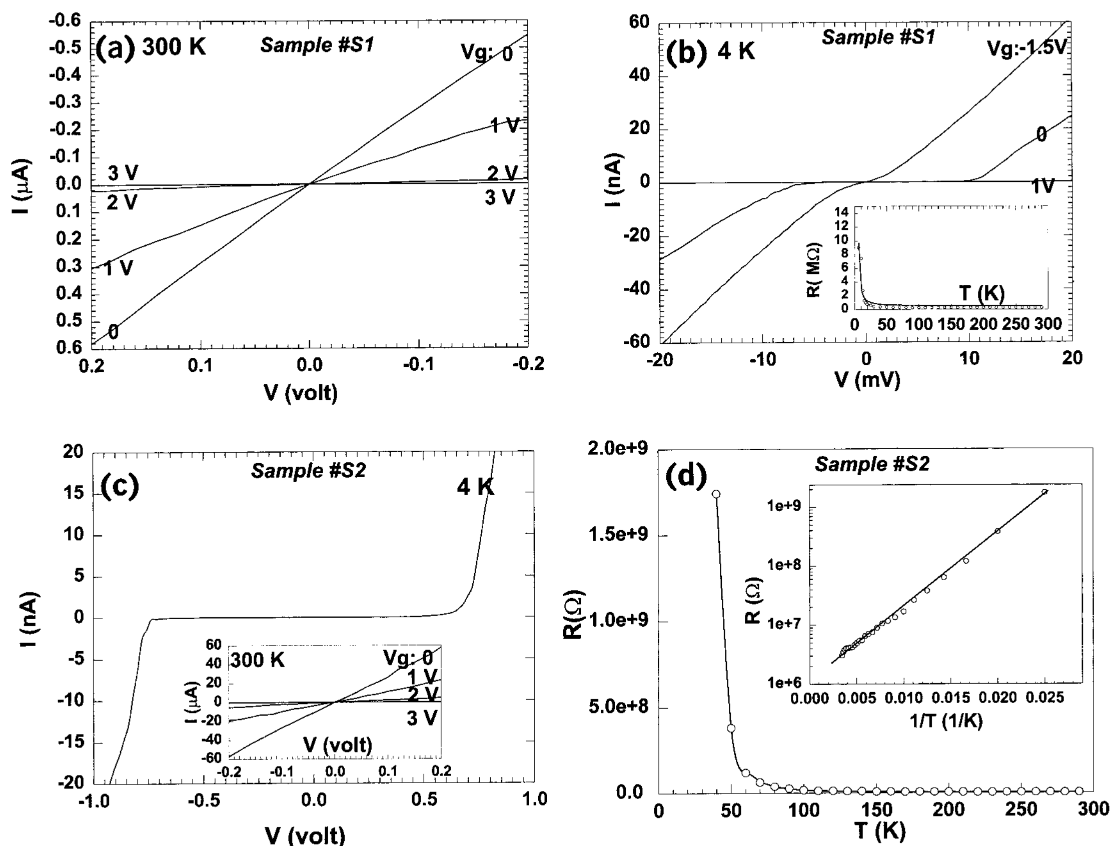

Figure 7. (a) Room-temperature $I-V$ characteristics of a $d = 2.8$ nm semiconducting SWNT (sample S1) contacted by 20 nm/60 nm Ni/Au. (b) $I-V$ curves recorded at 4 K for sample S1 under various gate voltages (inset: linear resistance vs temperature). (c) $I-V$ curve for a $d = 1.3$ nm semiconducting SWNT (sample S2) with Ni contacts recorded at 4 K (inset: room-temperature $I-V$ characteristics). (d) Linear resistance vs temperature (inset: plot of resistance in log scale vs $1/T$).

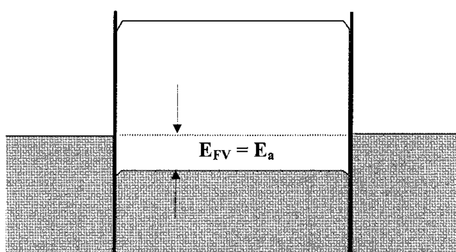

Figure 8. Proposed band diagram for a metal−semiconducting SWNT−metal system. The junction barrier height E_a is determined by the separation between the nanotube Fermi level and the valence band $E_{FV} = E_F - E_V$.

transport results. First, we consider that the nanotube is uniformly hole-doped along its entire length. Hole-doping to nanotubes was previously attributed to electron transfer from nanotubes to metal electrodes due to different work functions.[10] In our samples, it is not plausible that the effect of work function mismatch ($\phi_{Ni} = 5.5$ eV vs $\phi_{NT} \approx 4.5$ eV) can extend over the $\sim$3−5 μm long tube. Furthermore, we have used titanium, aluminum, and silver, which have similar work functions as graphite, and magnesium and calcium with lower work functions than graphite for the contacting metals. The resulting semiconducting tube samples all appear to be hole-doped and show p-type transistor behavior. Thus, metal/tube work function mismatch does not appear to be the origin of hole-doping in our samples. Nevertheless, a complete understanding of the precise doping mechanism requires further investigation. We tentatively propose that a possible doping source could be charged species on the sample surface or trapped charges in the substrate near the SWNT. Stray or trapped charges are known to exist in SiO_2/Si systems and affect the electrical characteristics of conventional semiconductor devices.[66] It is also possible that interactions between a nanotube and molecular species in the environment (including surface hydroxyl groups and other species on the SiO_2) lead to the observed hole-doping effects. Such doping mechanisms act over the entire length of a nanotube instead of being localized near the contacts. Note that homogeneous hole-doping to SWNTs was also suggested in ref 11. Second, we suggest that each contact consists of a series resistance (black bar in Figure 8) and forms a Schottky-like junction with the p-type nanotube bridge. The junction barrier height approximately equals the separation between the nanotube Fermi level and the valence band $E_{FV} = E_F - E_V$.

The junction barrier is responsible for the observed thermally activated transport through semiconducting SWNTs and is determined to be $E_a \approx E_{FV} \approx 4.6$ and 25 meV respectively for samples S1 and S2. The expected energy gap for the $d = 2.8$ and 1.3 nm length tubes are $E_g \approx 0.2$ and 0.6 eV, respectively, according to band structure calculations. Thus, the semiconducting tubes are hole-doped to large degrees. At 300 K, the samples exhibits linear $I-V$ curves (under zero gate voltage), since the junction barriers can be overcome by thermal energy $E_a \leq k_BT = 26$ meV. Positive gate voltages cause the valence band to shift down from the Fermi level, leading to higher barriers and thus less conducting states as seen in parts a and c of Figure 7. At 4 K where $k_BT \ll E_a$, thermally activated transport through the system is quenched. The sample is in an insulating state near zero bias, as shown in parts b and c of Figure 7. Under significantly high bias voltages, the sample is turned into a conducting state. Analyses of the $I-V$ curves (Figure 7b,c) indicate that current increases by $\sim$3 orders of magnitude after

the turn-on and can be fitted to $I \sim \exp(-c/V)$ where c is a constant. These results suggest that electron transport through a semiconducting tube at low temperatures is via a tunneling mechanism. Under a high bias voltage, electron tunneling occurs through the reverse biased Schottky-like junction. The mechanism of thermally activated transport at high temperatures and transport via tunneling at low temperatures is similar to that observed in conventional metal−semiconductor−metal systems by Lepselter and Sze.[65]

Integrated Nanotube Devices

Nanotube Molecular Transistors with High Gains. Previous single-walled nanotube (SWNT) field effect transistors (FET) obtained by randomly deposited SWNTs across electrodes exhibit low transconductance and voltage gain.[10,11] Our controlled chemical synthesis and integration approach have led to single-walled nanotube transistors that "mimic" silicon-based metal oxide field effect transistors (MOSFET) with similar $I-V$ characteristics and normalized transconductance. First, with our semiconducting nanotube samples, we reproducibly observed an interesting feature in the $I-V$ curves when high bias voltages were applied. The $I-V$ curves show marked asymmetry with respect to the polarity of the bias voltage when $|V| \geq 1$ V. $I-V$ curves obtained at room temperature with the $d = 2.8$ nm tube sample (S1) over a bias range of 3 to −3 V are presented in Figure 9a. Under a given gate voltage, the absolute current value is higher under a positive bias than under its negative bias. In the negative bias side, the current initially scales linearly as $|V|$ but reaches saturation and stays constant at large negative biases. On the positive bias side, the current increases monotonically as the bias voltage increases and does not show any saturation. The asymmetry in $I-V$ becomes increasingly dramatic under higher gate voltages. At $V_g = 3$ V, the $I-V$ curve essentially resembles that of a rectifying diode.

The asymmetry in $I-V$ is found to be inherent to the metal−tube−metal system. $I-V$ curves recorded after exchanging the source and drain electrodes show nearly unchanged asymmetry. Positive bias voltages still lead to higher absolute current values than negative biases (Figure 9b). Furthermore, we find that symmetrical $I-V$ curves can be obtained (Figure 9c) by scanning V in the range −3 to 3 V while biasing the two electrodes at $-V/2$ and $+V/2$, respectively. These results suggest that the observed asymmetrical $I-V$ curves are not caused by asymmetrical parameters such as different contact resistances at the two metal−tube interfaces. We conclude that for a significantly high bias voltage V, the current flow $|I|$ is not solely determined by the absolute value of voltage $|V|$ across the system and can be influenced by the bias configuration. The [0, $|V|$] bias configuration leads to higher current flow than the [0, $-|V|$] configuration; such asymmetry is introduced into the system by the large applied bias voltage. Note that asymmetry is nearly absent in the $I-V$ curves in the small bias regime ($|V| < 0.1$) as can be seen in Figure 7a.

The bias polarity associated asymmetrical $I-V$ has been consistently observed in all the p-type semiconducting SWNT samples that we have studied. We propose that the asymmetry in $I-V$ is caused by local gating effects of the biased drain electrode. Under a given gate voltage, the nanotube can be considered to have a constant hole density along its length. Under a negative bias configuration [0, $-|V|$], the electric field lines can be substantially enhanced at the nanotube section near the drain electrode for $|V| \geq 1$ V. The negative drain bias effectively introduces an increase in the gate voltage localized near the tube section close to the drain, resulting in a reduction

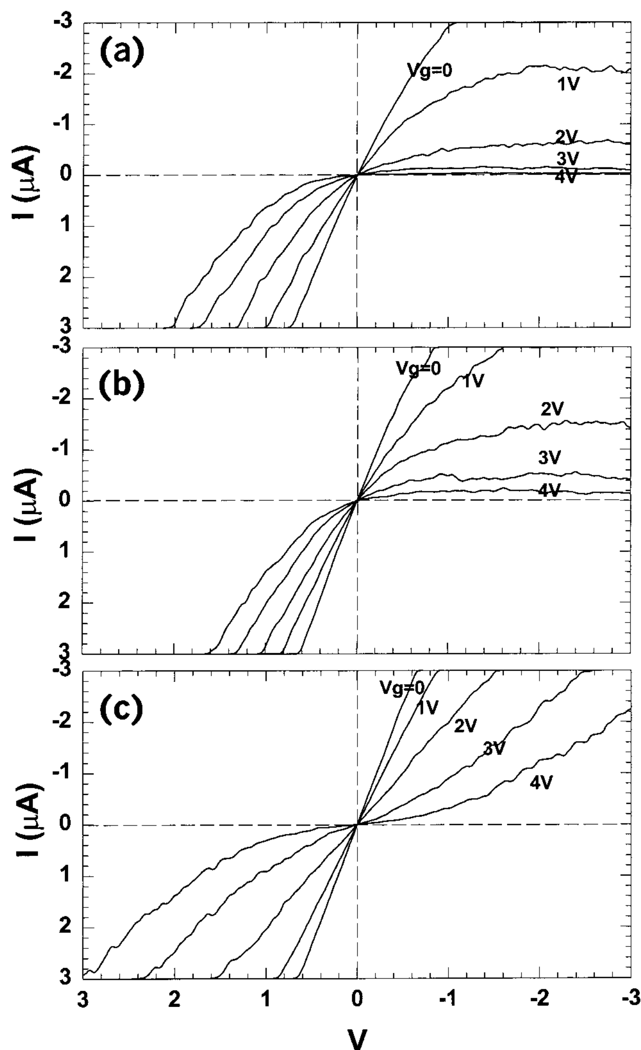

Figure 9. (a) Room-temperature $I-V$ curves recorded with sample S1 for V in the range 3 to −3 V under various gate voltages. (b) $I-V$ curves recorded after exchanging the source−drain electrodes. (c) Symmetrical $I-V$ curves obtained by scanning V while biasing the two electrodes at $-V/2$ and $V/2$, respectively.

of hole density in the section. Equivalently, a higher barrier to transport resulted at the junction at the drain. The $I-V$ curve thus falls below the line extrapolated from the low-bias curve. Saturation occurs in the $I-V$ curve for large $|V|$ because of the competing roles of driving and gating of the drain bias voltage. On the other hand, under the positive bias configuration [0,$|V|$], the electric field lines at the section of the nanotube close to the drain becomes suppressed or even reversed at large $|V|$. This leads to local hole enrichment (or equivalently barrier lowering) in the nanotube section near the drain, and the $I-V$ curve deviates to the higher current direction from the linear curve extrapolated from the small bias regime. Overall, a negative or positive bias voltage with absolute value on the order of ~1 V locally depletes or increases the hole-carrier density in the nanotube segment near the drain, leading to a lower absolute current level when the system is negatively biased. This phenomenon can be related to local carrier depletion and channel pinch-off by negative drain bias in a conventional p-type MOSFET.[66]

Our results are significant in the realization of high-performance nanotube-based transistors. First, the $I_{ds}-V_{ds}$ curves of our samples exhibit similar characteristics as silicon-based devices.[66] Second, high voltage gain and transconductance are

obtainable with our samples. Sample S1 (Figure 9) exhibits positive voltage gain of $\Delta V_{ds}/\Delta V_g|_{I=3\mu A} \approx 3$ compared to the maximum gain of ~0.35 obtained previously.[10] From the linear region of the $I_{ds} - V_{ds}$ curves, we derive a transconductance $\partial I_{ds}/\partial V_g|_{V=100mV} \approx 200$ nA/V, which is 2 orders of magnitude higher than previous results with SWNTs.[11] Normalized by the diameter of the nanotube ("channel width"), the transconductance is ~0.1 mS/μm and is comparable to that of a silicon p-MOSFET.

Conclusion

This article presented synthetic strategies that lead to various nanotube architectures useful for fundamental studies and potential applications of nanotube wires. Undoubtedly, the approach of direct growth of nanowire materials into ordered structures represents a promising direction toward new nanoscale science and devices. This method achieves atomically well-defined nanowires by bottom−up chemical routes, and wired-up architectures that normally require top−down fabrication or assembly techniques. The general approach of chemical vapor deposition has received considerable attention recently because of the unique opportunities in scaling up nanotubes in bulk and organizing nanowires on large-scale surfaces. Ordered multi-walled nanotube architectures can now be synthesized by several CVD methods on various substrates. The structured nanotube materials can be scaled up in straightforward ways and shall find applications in electron field emission, flat panel display, large-scale scanning force probes, electrochemical sensors, and electrodes. Single-walled carbon nanotubes are unique because their diameters enter a regime such that their electrical properties is strongly manifested by quantum confinement effects in the other two dimensions and their structures on the atomic scale. It can be envisioned that in the foreseeable future, SWNT architectures will be integrated as key components into microchips of next generations of electronic, memory, logic, mechanical, and electromechanical devices.

Significant future work is required in order to meet the continued challenge in controlled nanotube synthesis. It is desired to gain the full ability to grow SWNTs at any desired location with controlled orientations, either on flat or textured surfaces or at the ends of scanning probes or at any other places. It is an ultimate synthetic goal if one can control whether a semiconducting or metallic SWNT is grown at a particular location with directionality. Controlling the atomic structure of nanotubes including diameter and chirality probably will require the development of catalytic particles with molecularly well-defined structures. Thus, one of the main focuses in future research should be the development of new catalyst materials and catalyst support materials. Also, a deeper understanding of the chemistry of catalyst and nanotube growth is required. We are convinced that further control in nanotube synthesis will continue to open new possibilities in nanoscale science and technology.

Acknowledgment. We thank C. Quate, H. Soh, J. Han, C. Marcus, and A. Morpurgo for discussions and collaboration. This work was supported by National Science Foundation Partnership for Nanotechnology (ECS-9871947), Laboratory for Advanced Materials (LAM) at Stanford, a Terman Fellowship, Semiconductor Research Corporation, National Nanofabrication Users Network (funded by National Science Foundation ECS-9731294), the Camile Henry-Dreyfus Foundation, American Chemical Society, DARPA/ETO, and DARPA/Navy.

References and Notes

(1) Dresselhaus, M. S.; Dresselhaus, G.; Eklund, P. C. *Science of Fullerenes and Carbon Nanotubes*; Academic Press: San Diego, CA, 1996; Vol. 1, p 985.
(2) Ebbesen, T. W. *Phys. Today* **1996**, *49*, 26−32.
(3) Yakobson, B. I.; Smalley, R. E. *Am. Sci.* **1997**, *85*, 324−337.
(4) Dekker, C. *Phys. Today* **1999**, *52*, 22−28.
(5) Dai, H. J.; Hafner, J. H.; Rinzler, A. G.; Colbert, D. T.; Smalley, R. E. *Nature* **1996**, *384*, 147−150.
(6) Dai, H.; Franklin, N.; Han, J. *Appl. Phys. Lett.* **1998**, *73*, 1508−1510.
(7) Wong, S.; Joselevich, E.; Woolley, A.; Cheung, C.; Lieber, C. *Nature* **1998**, *394*, 52−55.
(8) Wong, S.; Harper, J.; Lansbury, P.; Lieber, C. M. *J. Am. Chem. Soc.* **1998**, *120*, 603−604.
(9) Hafner, J.; Cheung, C.; Lieber, C. *Nature* **1999**, *398*, 761−762.
(10) Tans, S.; Verschueren, A.; Dekker, C. *Nature* **1998**, *393*, 49−52.
(11) Martel, R.; Schmidt, T.; Shea, H. R.; Hertel, T.; Avouris, P. *Appl. Phys. Lett.* **1998**, *73*, 2447−2449.
(12) Soh, H.; Morpurgo, A.; Kong, J.; Marcus, C.; Quate, C.; Dai, H. *Appl. Phys. Lett.* **1999**, 75.
(13) de Heer, W. A.; Chatelain, A.; Ugarte, D. *Science* **1995**, *270*, 1179−1180.
(14) Bonard, J.-M.; Salvetat, J.-P.; Stöckli, T.; Heer, W. A. d.; Forró, L.; Châtelain, A. *Appl. Phys. Lett.* **1998**, *73*, 918−920.
(15) Collins, P. G.; Zettl, A. *Appl. Phys. Lett.* **1996**, *69*, 1969−1971.
(16) Saito, Y.; Hamaguchi, K.; Hata, K.; Tohji, K. *Ultramicroscopy* **1998**, *73*, N1-4:1-6.
(17) Wang, Q.; Setlur, A.; Lauerhaas, J.; Dai, J.; Chang, R. H. *Appl. Phys. Lett.* **1998**, *72*, 2912−2913.
(18) Fan, S.; Chapline, M.; Franklin, N.; Tombler, T.; Cassell, A.; Dai, H. *Science* **1999**, *283*, 512−514.
(19) Iijima, S. *Nature* **1991**, *354*, 56−58.
(20) Li, W. Z.; Xie, S. S.; Qian, L. X.; Chang, B. H.; Zou, B. S.; Zhou, W. Y.; Zhao, R. A.; Wang, G. *Science* **1996**, *274*, 1701−1703.
(21) Pan, Z.; Xie, S. S.; Chang, B.; Wang, C. *Nature* **1998**, *394*, 631−632.
(22) Ren, Z. F.; Huang, Z. P.; Xu, J. W.; Wang, J. H. *Science* **1998**, *282*, 1105−1107.
(23) Iijima, S.; Ichihashi, T. *Nature* **1993**, *363*, 603−605.
(24) Che, G.; Lakshmi, B.; Fisher, E.; Martin, C. *Nature* **1998**, *393*, 346−349.
(25) Kyotani, T.; Tsai, L. F.; Tomita, A. *Chem. Mater.* **1996**, *8*, 2109−2113.
(26) Vial, J.-C.; Derrien, J. In *Porous silicon science and technology: winter school, Les Houches, 8 to 12 February, 1994*.
(27) Smith, R. L.; Collins, S. D. *J. Appl. Phys.* **1992**, *71*, R1−R22.
(28) Bethune, D. S.; Kiang, C. H.; DeVries, M.; Gorman, G.; Savoy, R.; Vazquez, J.; Beyers, R. *Nature* **1993**, *363*, 605−607.
(29) Journet, C.; Maser, W. K.; Bernier, P.; Loiseau, A.; Delachapelle, M. L.; Lefrant, S.; Deniard, P.; Lee, R.; Fischer, J. E. *Nature* **1997**, *388*, 756−758.
(30) Thess, A.; Lee, R.; Nikolaev, P.; Dai, H. J.; Petit, P.; Robert, J.; Xu, C. H.; Lee, Y. H.; Kim, S. G.; Rinzler, A. G.; Colbert, D. T.; Scuseria, G. E.; Tomanek, D.; Fischer, J. E.; Smalley, R. E. *Science* **1996**, *273*, 483−487.
(31) Tibbetts, G. G. *Appl. Phys. Lett.* **1983**, *42*, 666−668.
(32) Tibbetts, G. G. In *Carbon Fibers, Filaments and Composites*; Figueiredo, J. L., Ed.; Kluwer Academic: Dordrecht 1990.
(33) Endo, M. *Chemtech* **1988**, 568−576.
(34) Baker, R. T. K.; Rodriguez, N. M. In *Symposium of the Materials Research Society*; Materials Research Society, 1994; Vol. 349, pp 251−256.
(35) Snyder, C. E.; Mandeville, W. H.; Tennent, H. G.; Truesdale, L. K. Int. Patent WO 89/07163, 1989.
(36) Kong, J.; Cassell, A. M.; Dai, H. *Chem. Phys. Lett.* **1998**, *292*, 567−574.
(37) Kong, J.; Soh, H.; Cassell, A.; Quate, C. F.; Dai, H. *Nature* **1998**, *395*, 878.
(38) Cassell, A.; Raymakers, J.; Kong, J.; Dai, H. *J. Phys. Chem. B* **1999**, *103*, 6484−6492.
(39) Tibbetts, G. G.; Devour, M. G.; Rodda, E. J. *Carbon* **1987**, *25*, 367−375.
(40) Tibbetts, G. G. *J Cryst. Growth* **1984**, *66*, 632−638.
(41) Baker, R. T. K. *Carbon* **1989**, *27*, 315−323.
(42) Amelinckx, S.; Zhang, X. B.; Bernaerts, D.; Zhang, X. F.; Ivanov, V.; Nagy, J. B. *Science* **1994**, *265*, 635−639.
(43) Kong, J.; Zhou, C.; Morpurgo, A.; Soh, T.; Marcus, C.; Quate, C.; Dai, H. *Appl. Phys. A* **1999**, *69*, 305−308.
(44) Yang, P.; Deng, T.; Zhao, D.; Feng, P.; Pine, D.; Chmelka, B. F.; Whitesides, G. M.; Stucky, G. D. *Science* **1998**, *282*, 2244−2246.

(45) Yang, P.; Zhao, D.; Margolese, D.; Chemelka, B.; Stucky, G. *Nature* **1998**, *396*, 152.

(46) Xia, Y.; Whitesides, G. M. *Angew. Chem., Int. Ed.* **1998**, *37*, 551−575.

(47) Ferguson, G.; Chaudhury, M.; Sigal, G.; Whitesides, G. M. *Science* **1991**, *253*, 776−778.

(48) Saito, R.; Fujita, M.; Dresselhaus, G.; Dresselhaus, M. S. *Appl. Phys. Lett.* **1992**, *60*, 2204.

(49) Mintmire, J. W.; Dunlap, B. I.; White, C. T. *Phys. Rev. Lett.* **1992**, *68*, 631−634.

(50) Hamada, N.; Sawada, S.; Oshiyama, A. *Phys. Rev. Lett.* **1992**, *68*, 1579−1581.

(51) Odom, T.; Huang, J.; Kim, P.; Lieber, C. M. *Nature* **1998**, *391*, 62−64.

(52) Wildoer, J. W. G.; Venema, L. C.; Rinzler, A. G.; Smalley, R. E.; Dekker, C. *Nature* **1997**, *391*, 59−62.

(53) Tans, S. J.; Devoret, M. H.; Dai, H.; Thess, A.; Smalley, R. E.; Geerligs, L. J.; Dekker, C. *Nature* **1997**, *386*, 474−477.

(54) Bockrath, M.; Cobden, D. H.; McEuen, P. L.; Chopra, N. G.; Zettl, A.; Thess, A.; Smalley, R. E. *Science* **1997**, *275*, 1922−1925.

(55) Cobden, D. H.; Bockrath, M.; Chopra, N. G.; Zettl, A.; McEuen, P. L.; Rinzler, A.; Smalley, R. E. *Phys. Rev. Lett.* **1998**, *81*, 681−684.

(56) Tans, S.; Devoret, M.; Groeneveld, R.; Dekker, C. *Nature* **1998**, *394*, 761−764.

(57) Bockrath, M.; Cobden, D.; Lu, J.; Rinzler, A.; Smalley, R.; Balents, L.; McEuen, P. *Nature* **1999**, *397*, 598−601.

(58) Kane, C.; Balents, L.; Fisher, M. P. A. *Phys. Rev. Lett.* **1997**, *79*, 5086−5089.

(59) White, C. T.; Todorov, T. N. *Nature* **1998**, *393*, 240.

(60) Kane, C. L.; Mele, E. J.; Lee, R.; Fischer, J. E.; Petit, P.; Dai, H.; Thess, A.; Smalley, R. E.; Verschueren, A. R. M.; Tans, S. J.; Dekker, C. *Eur. Phys. Lett.* **1998**, *6*, 683−688.

(61) Kane, C. L.; Mele, E. J. *Phys. Rev. Lett.* **1997**, *78*, 1932−1935.

(62) Chico, L.; Benedict, L. X.; Louie, S. G.; Cohen, M. L. *Phys. Rev. B* **1996**, *54*, 2600−2606.

(63) Tersoff, J. *Appl. Phys. Lett.* **1999**, *74*, 2122−2124.

(64) Morpurgo, A.; Kong, J.; Marcus, C.; Dai, H. *Science* **1999**, *286*, 263−265.

(65) Lepselter, M. P.; Sze, S. M. *Proc. IEEE* **1968**, *56*, 1400−1402.

(66) Sze, S. M. *Physics of semiconductor devices*; Wiley: New York, 1981.

(67) Rochefort, A.; Lesage, F.; Salahub, D.; Avouris, P. Preprint at http://xxx.lanl.gov/abs/cond-mat/9904083.

(68) Cassell, A.; Franklin, N.; Tombler, T.; Chan, E.; Han, J.; Dai, H. *J. Am. Chem. Soc.* **1999**, *121*, 7975−7976.